Acta Materialia 183 (2020) 242–248

Contents lists available at ScienceDirect

Acta Materialia

journal homepage: www.elsevier.com/locate/actamat

Full length article

Intrinsic toughness of the bulk-metallic glass Vitreloy 105 measured using micro-cantilever beams

Daniel Sorensen[a,b,*], Eric Hintsala[c], Joseph Stevick[d], Jesse Pischlar[a], Bernard Li[a], Daniel Kiener[e], Jason C. Myers[f], Hui Jin[a], Jia Liu[a], Douglas Stauffer[c], Antonio J. Ramirez[b], Robert O. Ritchie[g]

[a] Medtronic PLC, Minneapolis, MN 55432, USA
[b] Department of Materials Science and Engineering, Ohio State University, Columbus, OH 43221, USA
[c] Bruker, Eden Prairie, MN 55344, USA
[d] Liquidmetal Technologies, Lake Forest, CA 92630, USA
[e] Department of Materials Science, Montanuniversität Leoben, Leoben, Austria
[f] University of Minnesota Characterization Facility, Minneapolis, MN 55455, USA
[g] Materials Sciences Division, Lawrence Berkeley National Laboratory, and Department of Materials Science and Engineering, University of California, Berkeley, CA 94720, USA

ARTICLE INFO

Article history:
Received 9 May 2019
Revised 4 November 2019
Accepted 6 November 2019
Available online 11 November 2019

Keywords:
Bulk-metallic glasses
Fracture toughness
Micro-cantilever testing
Length-scale dependence

ABSTRACT

Bulk-metallic glasses (BMGs) are a class of structural materials with many attractive processing features such as the ability to be processed into parts with fine features, dimensional precision, and repeatability; however, their fracture behavior is complex and size-dependent. Previous work has shown that BMGs can display strong size effects on toughness, where multiple mechanisms on different length-scales, *e.g.*, crack bridging and bifurication, shear band spacing and length, can significantly affect the properies. This length-scale dependence on the fracture toughness has importance not only for advancing the understanding of fracture processes in these materials, but also for the potential future applications of BMGs, such as for microdevices. Here, using *in situ* scanning electron microscopy (SEM), we report on notched micro-cantilever bending experiments to address the lack of data regarding fracture properties of BMGs at the microscale. Sudden catastrophic propagation of shear bands resulted in failure for these specimens at stress intensities much lower than the bulk material, which may be due to a lack of extrinsic toughening mechanisms at these dimensions. This is explored further with *post mortem* SEM and transmission electron microscopy (TEM) analysis of the fractured beams while the fracture toughness results are verified using finite element modeling. The excellent agreement between model and micro cantilever beam bending experiments suggests that the intrinsic fracture toughness of Vitreloy 105, 9.03 ± 0.59 MPa.m^{½}, is being reported for the first time.

1. Introduction

Bulk-metallic glasses (BMGs) are a relatively new class of engineering materials with many desireable properties such as high elastic limit, low elastic modulus, good corrosion resistance, and the ability to be formed using injection molding into near-net shapes [1]. One of the largest issues limiting their widespread use is the inconsistency in their fracture toughness which has been shown to vary with part dimensions [2,3], material processing, and composition [4,5]. The fatigue (and therefore crack propagaton and toughness) properties of Vitreloy 1 [6-8] and Vitreloy 106a [9] have been studied and found to have similar stress intensity threshold limits and enviromental sensitivity to fatigue crack growth. Vitreloy 105 has been reported to have a higher fatigue threshold in four-point bending [10–11] than both Vitreloy 1 and 106a but does not share their sensitivity to test enviroment on fatigue crack growth rates. The unique mechanical properies, superior fatigue resistance, corrosion resistance and lack of beryllium make Vitreloy 105 an excellent candidate for use in engineering applications.

Many researchers have related such variations in fracture toughness on milli- to macro length-scale parts [6,7] to deformation and shear band formation at the sub-micrometer and

* Corresponding author at: Department of Materials Science and Engineering, Ohio State University, Columbus, OH 43221, USA.
E-mail address: sore0256@umn.edu (D. Sorensen).

https://doi.org/10.1016/j.actamat.2019.11.021
1359-6454/

nano scales [12–18]. Numerous groups have reported size effects in micropillar compression testing of bulk-metallic glasses where measurements on sub-micrometer pillars repeatibly gave higher yield stresses than pillars larger than 1000 nm [12–15] which was attributed to the higher probability of defects that aid in the formation of shear bands in larger samples. Other researchers have found the compression strength to be size-independent [16,17] with homogeneous flow not observed even in sub-micrometer samples. The combination of size effect, shear band formation, geometrically unfavored motifs [19], and impurities on the engineering performance of bulk-metallic glasses makes the fracture and fatigue behavior of bulk-metallic glasses an active area of research.

Recent investigations into the fracture and fatigue properties of high toughness, highly damage tolorant, palladium and zirconium-based bulk-metallic glasses have been published [3,20]. These studies also report the large effect of sample size on fracture toughness where larger scale samples fracture in a catostrophic brittle fashion while samples below critical bending thickness values experienced stable crack growth and R-curve behavior [3].

The ability to fabricate bulk metallic glasses with thicknesses of tens of micrometers creates numerous possible engineering applications that include MEMS devices [21], foils for sensors [22], leaf valves [23], springs [24], and hinges [25]. However, to the authors' best knowledge, no data on fracture properties exists at the micrometer length-scale for BMGs, which is required for any eventual commercial development of engineered components.

Here we report on the failure analysis and fracture toughness of micrometer-scale specimens for a commercially available Zr-based bulk-metallic glass, Vitreloy 105, using *in situ* micro cantilever beam bending, *post mortem* SEM fractograhy, TEM analysis and finite element modeling. Comparison of our results to nanoscale and millimeter scale studies is utilized to achieve a more comprehensive understanding of length-scale effects on the toughness and mechanical performance of these amorphous materials.

2. Experimental

The material used for this experiment was a 0.9 mm thick plate of Zr-based bulk-metallic glass (Vitreloy 105) with a composition of Zr-14.8Cu-11.3Ni-3.6Al-3.2Ti-0.047Be-0.013Si in wt.%, measured by inductively coupled plasma-optical emission spectroscopy (ICP-OES). Sections of the plate were cut to 100 mm^2 samples by electrical discharge machining (EDM) and the part surfaces were ground and prepared to a 50 nm final polish using an Allied MultiPrep polishing system. The amorphous structure of the samples was confirmed using x-ray diffraction. The pentagonal microbeams were fabricated by Ga^+ ions at 30 kV using an FEI Scios field emission gun scanning electron microscope/focused ion beam (FEG SEM/FIB). Initial shape profiling was performed at probe currents starting at 65 nA progressively reducing to 1 nA and all surfaces were final polished using a 100-pA probe current. The side cuts were made using a 2° over tilt to minimize taper. The notches were fabricated using an ion beam accelerating voltage of 5 kV, probe current of 48 pA, and Z depth of 500 nm using a standard line pattern. The larger 5 kV probe created a line with a narrow parabolic shape and opening at the surface making material re-deposition less of an issue while achieving radii of curvature at the notch root on the order of 25 nm. The notch depth was targeted to be on the order of 1.0 μm to achieve notch depth to thickness (a/W) ratios of approximately 0.3. Fig. 1 shows a representative beam with critical dimensions labeled.

All testing was performed with a Hysitron PI-85 PicoIndenter *in situ* in a FEI Versa FEG SEM/FIB operating at 20 kV. All beams ($n = 10$) were loaded using a conical diamond milled to a 2 μm flat punch in displacement control mode at 20 nm s^{-1}. A representative

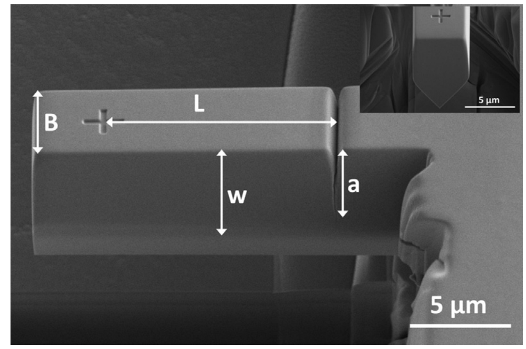

Fig. 1. SEM image of a representative Vitreloy 105 micro-cantilever beam with important dimensions labeled and end view shown in the inset.

Table 1
The material plastic hardening parameters used for FEA.

Yield Stress (MPa)	Plastic Strain
1950	0
3250	0.005

montage of images from an in situ experiment and their locations on the corresponding load-displacement curve are shown in Fig. 2.

Although fatigue and crack propagation of the Vitreloy 1 and 106a alloys have been reported to be sensitive to test environments ranging from ambient air to inert gasses [8,9], similar studies on Vitreloy 105 have shown the fatigue and fracture properties to be essentially independent of test environment [10]. This gives confidence that fracture toughness data collected inside the vacuum chamber of a FEG SEM over relatively short time scales are representative of samples tested in ambient conditions. Fracture surfaces of the failed samples were analyzed *post mortem* using an FEI Scios SEM operating at 5 keV. Samples for transmission electron microscopy (TEM) were lifted out from fractured beams using an FEI Scios FEG SEM/FIB fitted with an EasyLift system, prepared using a 2° overtilt for all polishing steps, and final polished using a 5 keV beam. TEM analysis was performed using an FEI Tecnai G^2 F30 operating at 300 keV.

Finite element analysis (FEA) was performed using Abaqus 6.14 commercial software. The beam model was discretized into second order hex 3D elements (Abaqus element type C3D20R). The mesh around the notch was highly refined to capture the stress gradient near the tip. The material constitutive law is assumed be to classical metal plasticity with isotropic hardening. Displacement control was applied to a reference point coupled with a small region on the beam, mimicking the contact between the indenter and the beam. To obtain the nonlinear-elastic energy release rate, the J integral method with 18 contours was applied in the model. The convergence of the contour integrals was monitored, and the converged value was readily taken as the energy release rate.

The linear elastic modulus was determined by nanoindentation and Poisson's ratio from [26] (85.6 GPa and 0.38, respectively). Excellent agreement can be seen for the linear regime, indicating that FEA model predicts faithfully the bending stiffness of the beam. Note that the material strain hardening inputs were tuned to capture the plastic behavior. These values were empirically chosen to fit the plastic region of the FEA load-displacement curve to the experimental results and to compare J values to the *in situ* tests for comparison purposes. The corresponding material parameters are listed in Table 1.

As a secondary check of the calculated J, we also compared it with the FEA predicted value, obtained from the center plane of the beam. To calculate the fracture energy and corresponding criti-

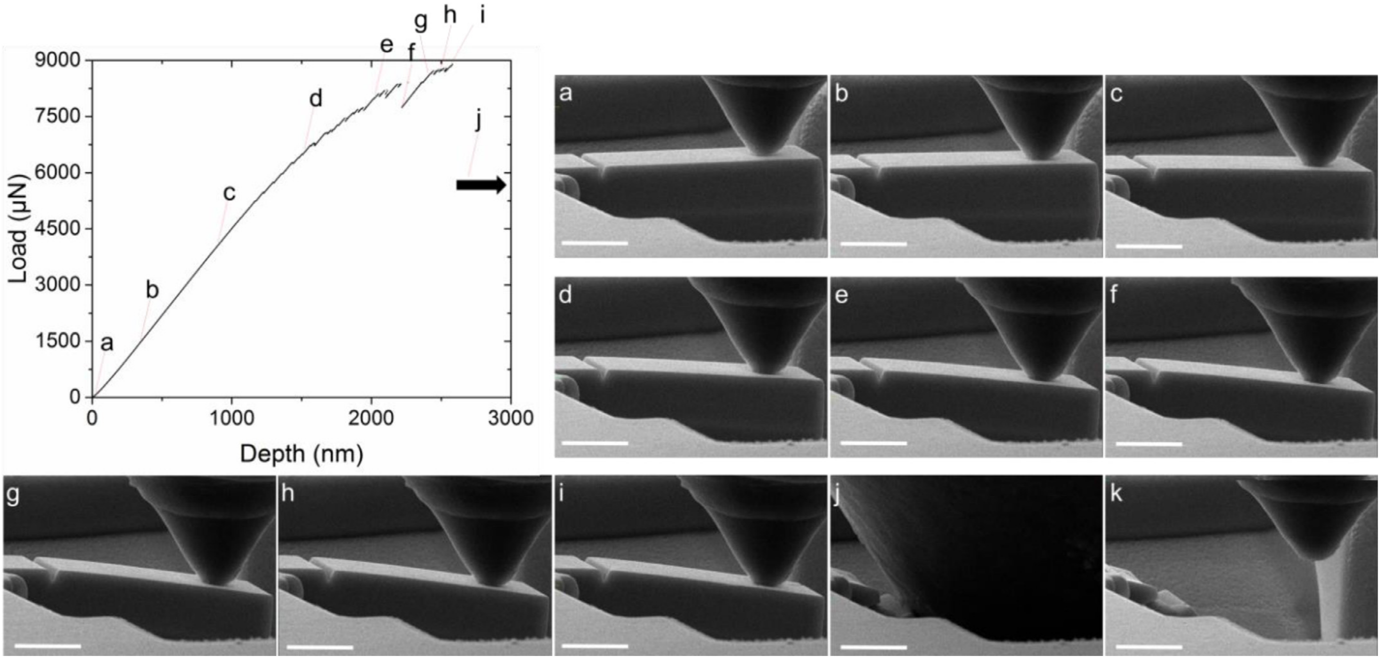

Fig. 2. Screen capture montage showing deformation of a representative Vitreloy 105 beam at several points on the load-displacement curve. The load drops (serrations) were confirmed to be the result of shear band propagation events during *post mortem* analysis. Scale bar signifies a length of 5 µm.

cal stress intensity factor, the simple fracture criterion $G > G_c$ was used, where G is the strain energy release rate and G_c is the critical value of G at fracture.

3. Results

Three distinct deformation regimes can be seen in the loading curves: elastic bending, limited plastic flow indicated by serrations in the load-displacement curve, and catastrophic failure. The serrated plastic flow was the result of shear band formation which was confirmed by *post mortem* analysis; also apparent was a constant loading stiffness prior to and immediately following the load drop, observation of opening of the notch flanks, and slight blunting of the crack tip. This type of shear band initiation was also found in previous research utilizing micro-indentation, nanoindentation, and nano pillar compression testing [27–29]. The combined results for all micro cantilever beam bending experiments, shown overlaid in Fig. 3a, display the same characteristics as Fig. 2, with a slight shift in load at the same displacement correlated with the notch length. The deviations observed in the elastic portion of the load-displacement curves appear to be random scatter or related to small variation in the loading location. Recordings of the *in situ* test revealed no unusual occurrences during the test.

To evaluate the fracture toughness from these data, first it is important to establish the regime that these tests are being conducted in. A linear-elastic fracture mechanics (LEFM) analysis was initially utilized to calculate the provisional critical stress intensity, K_Q, for the purposes of evaluating the plastic-zone size in relation to the specimen dimensions. To achieve this, the classic elastic cantilever solution Eqs. (1) and (2), similar to that used by Zhao et al. [30] and Di Maio and Roberts [31], was employed to compute the stress intensities as a function of load, crack size and sample dimensions. The results can be found in Table 2, along with estimates of the plastic-zone size, $r_y \sim 1/2\pi\ (K_Q/\sigma_y)^2$ calculated using the yield stress, σ_y, and elastic modulus, E, as determined by nanoindentation (1.95 GPa and 85.6 GPa), with the stress intensity K defined in terms of the applied stress σ for the cantilever bend geometry as [32]:

$$K = \sigma\sqrt{\pi a}\ f\left(\frac{a}{W}\right), \tag{1}$$

where

$$f\left(\frac{a}{W}\right) = 1.85 - 3.38\left(\frac{a}{W}\right) + 13.24\left(\frac{a}{W}\right)^2 - 23.26\left(\frac{a}{W}\right)^3 + 16.8\left(\frac{a}{W}\right)^4. \tag{2}$$

It can be observed from Table 2 that the measured linear-elastic fracture toughness was found to be $K_Q = 8.78\ \mathrm{MPa.m^{1/2}}$; using this value, the estimate of the plastic-zone size can be seen to exceed one tenth of both the beam width and the beam thickness, which indicates that the specimen dimensions did not meet the ASTM Standard 1820 [33] for fracture toughness testing with respect to both the K-field dominance of the crack-tip stress and displacement fields (small-scale yielding) and plane-strain constraint, respectively. Thus, the calculated values could not be strictly labeled as the fracture toughness K_c or plane-strain fracture toughness $K_{Ic,}$ in view of the small size of the samples [34]. Considering this, we employed a nonlinear-elastic fracture mechanics methodology to determine the critical value of the J-integral at fracture, J_{exp}, using measurements of the total work of fracture (involving elastic and plastic contributions), A_{cur}, and the specimen and crack size dimensions, as per ASTM Standard 1820 [33]. Specifically, this was calculated by integrating the area under the load-depth curves using Origin software to determine the mechanical work and then normalizing by the failed ligament cross-section, according to Eq. (3):

$$J = \frac{2A_{cur}}{(W-a)*B + \frac{B^2}{4}} \tag{3}$$

where W is the beam width and B the beam thickness. The calculated J value at fracture, $J_{Ic,exp}$, was found to be ~818 J.m^{-2}; the validity for this value, as per ASTM Standard 1820 in terms of the existence of plane strain and J-dominant crack-tip fields, can be achieved if respectively B and $(W\text{-}a) > 10\ J_{exp}/\sigma_{flow}$, where σ_{flow}

Table 2
Measured and computed average values with standard deviations of the provisional linear elastic fracture toughness, K_Q, plastic-zone size, r_y, and the nonlinear-elastic $J_{c,exp}$ fracture toughness and the critical stress intensity $K_{Jc,exp}$, back-calculated from this J value, and the critical stress intensity, $K_{Jc,exp}$ computed from the FEA analysis.

K_Q (MPa.m$^{1/2}$)	r_y (µm)	r_y/B	r_y/W	$J_{c,exp}$ (J.m^{-2})	$K_{Jc,exp}$ (MPa.m$^{1/2}$)	$K_{Jc,FEA}$ (MPa.m$^{1/2}$)
8.78±0.59	3.24±0.44	0.48±0.07	0.86±0.15	818.2 ± 101.9	9.03±0.59	9.55

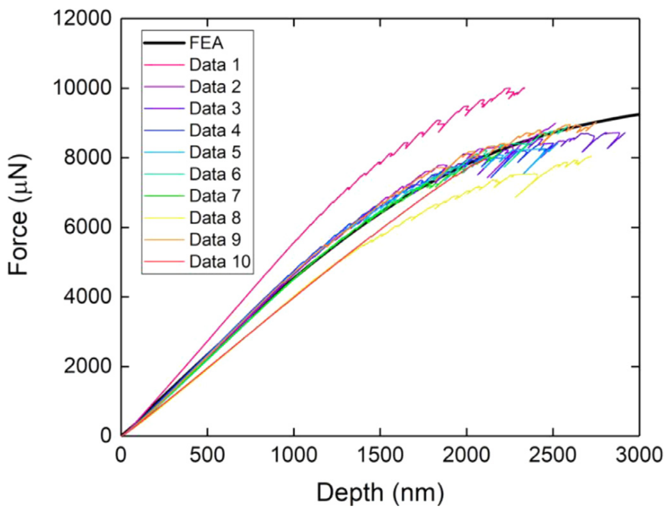

Fig. 3. Load-displacement curves for all 10 micro-cantilevers fractured in this study with overlaid FEA result. The deviations in the elastic regime of samples 1 and 8 were determined to be experimental noise as careful review of the *in situ* test video showed no apparent issues with samples 1 and 8 as compared to the other beams.

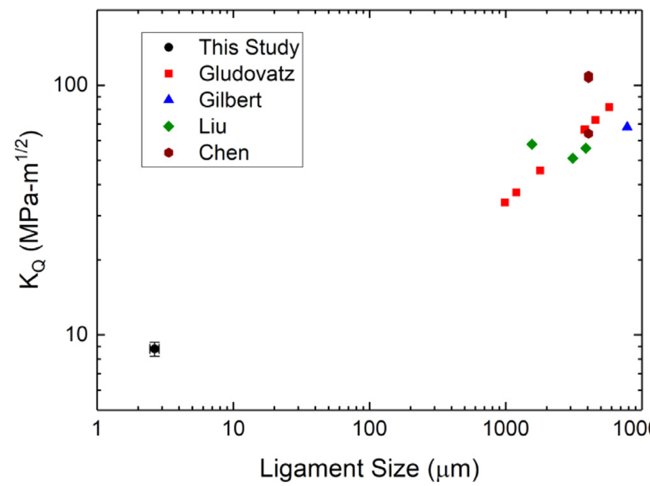

Fig. 4. Scatter plot of apparent fracture toughness K_Q as a function of the uncracked ligament length b comparing the results of this study on micrometer-scale samples to millimeter-sized samples reported by other groups: Gludovatz et al. [2], Gilbert et al. [7], Liu et al. [38], and Chen et al. [4]. The error bars on the microcantilever data signify 1 standard deviation from the mean.

is the average calculated bending stress of the cantilevers tested (3076 MPa). The condition for plane strain, that $B > 10\ J_{exp}/\sigma_{flow}$, was met for all experimental cases, but the more important ASTM requirement of J-dominance at the crack tip, that of $(W\text{-}a) > 10\ J_{exp}/\sigma_{flow}$, was strictly met only for 3 of the 10 conditions; as 7 of the 10 cases though were very close to this J-validity condition (*i.e.*, within 15%) and these size criteria tend to be quite conservative, we believe that all our measured $J_{Ic,exp}$ at fracture represent an accurate assessment of the plane-strain fracture toughness. A stress-intensity based fracture toughness, $K_{J,exp}$, was then back-calculated from the critical $J_{Ic,exp}$ value at fracture value, using the standard mode I K-J equivalence, *i.e.*, $J = K^2/E'$, where the Young's modulus value in plane strain is given in terms of Poisson's ratio ν (0.38) as $E' = E/(1 - \nu^2)$. The resulting J-based fracture toughness, $K_{Jc,exp}$, was found to be 9.03 MPa.m^{½}. Fig. 3 shows the force-displacement curves for 10 tested samples, superimposed by the FEA results. In the FEA model, the geometry was built using the measured mean dimensions of the 10 tested samples. At displacement of 2900 nm, energy release rate results from the FEA J integral analysis were found to converge at 0.91 N.mm^{-1} which agrees with our experimentally measured values of 0.818 N.mm^{-1}. Experimental test results indicate that fracture occurred at displacements of approximately 2900 nm. Therefore, the fracture energy obtained from FEA is 0.91 N.mm^{-1}, and critical stress intensity factor K_J from FEA is 9.55 MPa·m$^{1/2}$ *i.e.*, in excellent agreement with the experimental results. Furthermore, the von Mises stress contours (Fig. 5) in the deformed model agreed with the locations of shear band formation, plastic-zone size, and final fracture.

4. Discussion

The good agreement between the various experimental and numerical estimates of the fracture toughness of this metallic glass at the micrometer-scale, namely a slightly invalid LEFM experimental K_Q value of 8.78 MPa·m$^{1/2}$, a valid, plane-strain K_{Jc} value (determined experimentally using J-based measurements) of 9.03 MPa·m$^{1/2}$, and a numerically determined value (based on energy-release rates) of 9.55 MPa·m$^{1/2}$, supports the conclusion that the fracture toughness of these specimens has been realistically determined to be on the order of 10 MPa·m$^{1/2}$ at the micrometer-scale. This is to be contrasted with the toughness values reported in the literature for millimeter-sized samples of Vitreloy 1 [6,7] and Vitreloy 105 [2,4], where K_{Ic} values have been reported to be between 20–100 MPa·m$^{1/2}$, *i.e.*, between 2 and 10 times higher. Significant issues with size-effects on the toughness of BMGs have been reported for measurements on the millimeter scale [2] and on shear band formation down to hundreds of nanometers [17,18,35,36]. In general, smaller metallic glass samples were found to have relatively higher toughness due to a loss of plane-strain confinement as the sample size decreased to around 2 mm [2]. In fact, early millimeter-scale fracture tests resulted in what were considered surprisingly high fracture toughness values when compared against an estimate using the Taylor instability [6], which resulted in a value of 13 MPa·m$^{1/2}$, which approaches our experimental measurements here.

Fig. 4 compares the apparent fracture toughness values from this study plotted with results from recent work on the fracture toughness K_Q of Zr-based metallic glasses from other research groups. A trend of conditional fracture toughness decreasing as ligament length b decreases has been reported. Previous studies have shown a gradual increase in K_Q and marked improvements to toughness in bending as b decreases [2]. The observed low toughness values may be related to the primary shear bands propagating through the beam thickness resulting in fracture of the beam. Samples with larger geometries have been shown to have a high density of primary and secondary shear bands which propagate though the sample accommodating plastic flow [38]. In the current study, the calculated plastic-zone size is larger than the ligament length of our samples while the plastic zone size (either reported

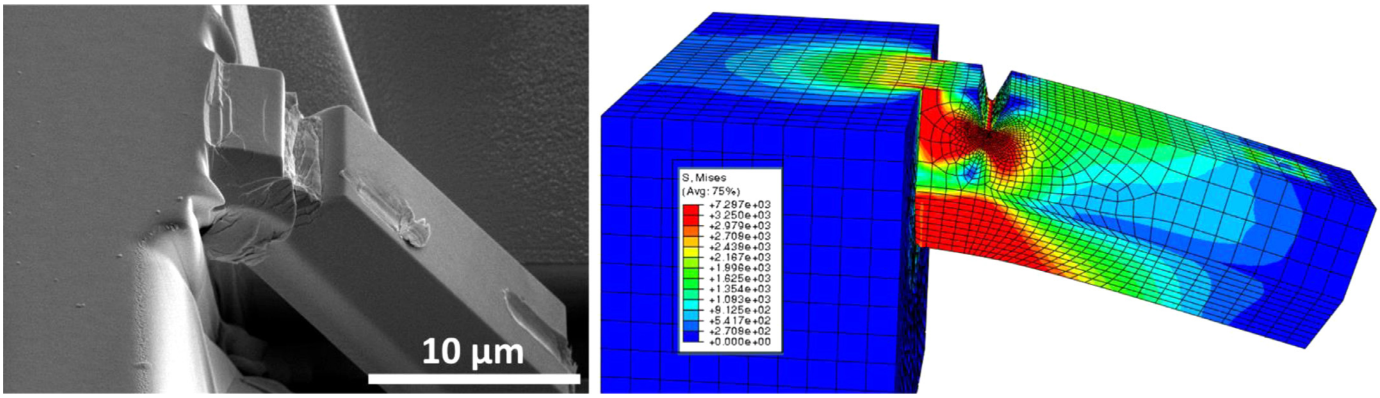

Fig. 5. (a) Fractograph showing a profile of a representative Vitreloy 105 beam following a catastrophic failure compared to (b) FEA model of a deformed Vitreloy 105 beam following a 2900 nm displacement at the end of the beam. Note the locations of the beam where shear banding and a large plastic zone were experimentally observed, correlating with the highest von Mises stresses as predicted in the model in units of MPa.

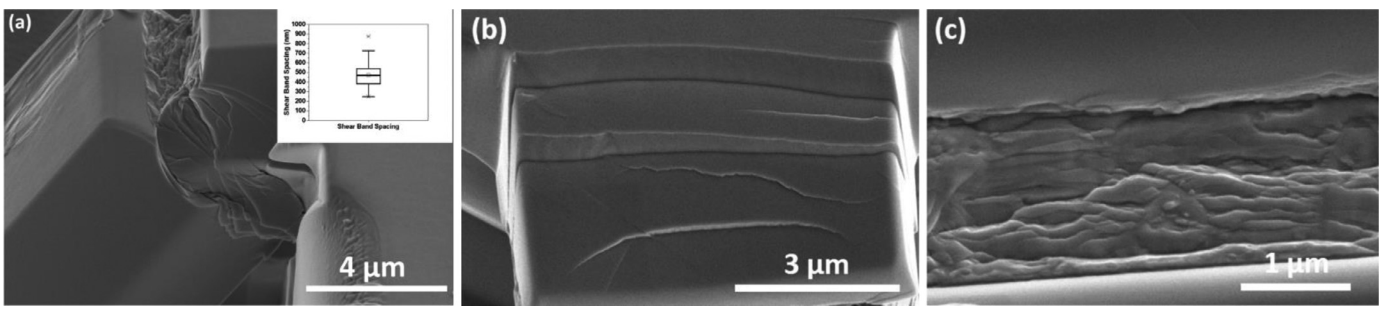

Fig. 6. Scanning electron micrograph showing shear banding and catastrophic brittle fracture in detail. Inset boxplot showing the shear band spacing distribution for all pentagonal beams tested in this study. High magnification SEM images showing (b) shear banding and (c) areas of apparent local melting on the fracture surface. No signs of microvoids or ductile rupture were observed on any samples tested.

or calculated from reported data) in the studies below reveal the plastic-zone size to be nearly an order of magnitude smaller than the ligament length for millimeter-scale samples [2,7,4,38].

Additionally, there has been concern over the extent of validity of *J*-based analysis for BMGs [2] due to their limited strain hardening [39], which would act to restrict the extent of the HRR-singularity of stress and displacement fields at the crack tip upon which the uniqueness of the *J*-field is based [40,41]. However, we do not believe that this is a major problem with the current values due to the similarity of the linear-elastic *K*-based and nonlinear-elastic *J*-based toughness estimates and their agreement with the numerically derived value. Since the results presented here represent a crack-initiation toughness only, *i.e.*, fracture occurred catastrophically with crack instability simultaneous with initiation, there is no evidence of stable cracking or crack-resistance R-curve behavior, which often is the basis of extrinsic toughening mechanisms,[1] such as the crack-bridging and deflection phenomena that clearly affects some of the higher values reported for the bulk scale [2]. Indeed, *post mortem* SEM and FEA analysis, shown in Fig. 5, demonstrate clearly that fracture occurred catastrophically in a volume approaching the thickness of the beam.

The fracture surface morphology of failed cantilevers indicate areas of local melting from shear band formation (Fig. 6), similar to that reported in ref. [27], with crack propagation associated with prototypical brittle fracture. The shear band spacing was on the order of 500 nm and followed the trend reported by Conner et al. where bending experiments of Zr-based metallic glass showed

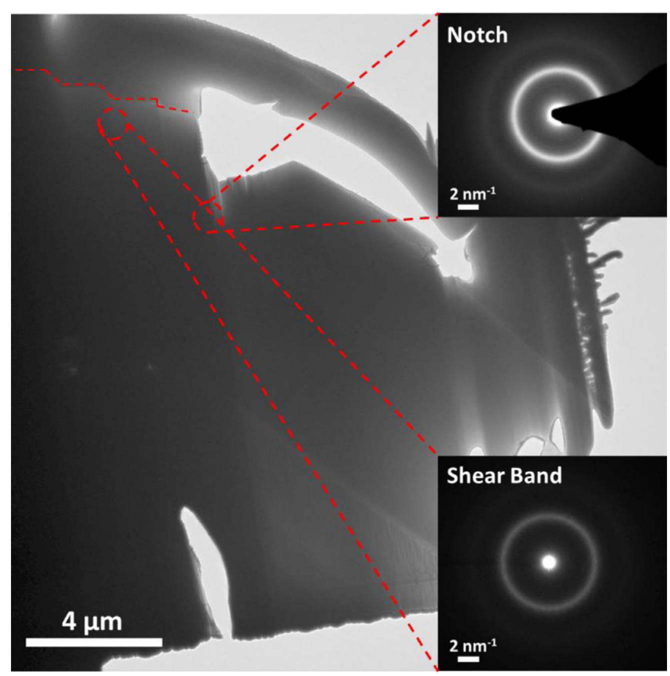

Fig. 7. Transmission electron micrograph with inset selected area diffraction patterns showing a lack of crystallization caused by FIB milling at the notch tip or local melting during shear band formation. The surface steps from the shear banding are highlighted by a dotted line.

[1] Fracture resistance can be considered as a mutual competition between two classes of toughening mechanisms: intrinsic mechanisms, which resist microstructural damage ahead of the crack tip and are motivated primarily by plasticity, and extrinsic mechanisms, which operate at, or in the wake of, the crack tip to inhibit fracture by "shielding" the crack from the applied driving force [42]. Whereas intrinsic toughening mechanisms are effective in inhibiting both the initiation and growth of cracks, extrinsic toughening mechanisms, such as crack bridging and crack deflection, are only effective in inhibiting crack growth.

shear band spacing decreased as sample size decreased [37]. Liu et al. and Suh et al. also reported a shear band spacing/sample geometry relationship resulting in brittle fracture when the sample geometry is decreased [43,44]. These observations agree with our *post mortem* analysis of primary shear band spacing seen in Fig. 6a–c.

Lastly, TEM samples prepared from failed beams showed no signs of crystallization at the notch root or within shear bands that may have impacted the toughness measurements. Rather, the TEM/selected area diffraction (SAD) analysis confirmed that the beam remained amorphous at the notch tip after ion beam fabrication as well as after final fracture as shown in Fig. 7.

From an engineering standpoint, our results that the micrometer-scale fracture toughness of bulk-metallic glasses may be up to an order of magnitude lower than corresponding values measured at the millimeter-scale are important, because components made from BMGs containing micro-meter scale features may not benefit from the toughening observed in larger samples. This markedly lower micrometer-scale toughness should be considered when designing small-scale components such as small-scale features, thin films, or MEMS devices using BMGs.

5. Conclusions

The fracture properties of micrometer-scale samples of Vitreloy 105 bulk-metallic glass show a size effect with a markedly different fracture toughness to that of milli- to macro-scale specimens, where high toughness and extrinsic toughening behavior have been observed. The analyses showed an average fracture toughness at crack initiation/instability ranged from 8.78 (K_Q LEFM measurements) to 9.03 (back-calculated from valid J-based measurements) MPa·m$^{1/2}$ and 9.55 MPa·m$^{1/2}$ (FEA-based energy-release rate simulation), values that are by a factor of 2 to 10 lower than measurements reported for this glass in the literature for larger-scale samples. Experimental observations and plastic-zone size calculations suggest the low fracture toughness is related to the cantilever dimensions being on the same order as the plastic zone, resulting in a small extent of plasticity in the form of the degree of shear banding prior to catastrophic failure, with no evidence of extrinsic toughening and resistance-curve behavior. These findings are critical for the further understanding size effect phenomena on the fracture toughness of the metallic glasses.

Declaration of Competing Interest

The authors declare that they have no known competing financial interests or personal relationships that could have appeared to influence the work reported in this paper.

Acknowledgments

The authors would like to acknowledge the Medtronic Restorative Therapies Group leadership for financial support of this research. D. Sorensen would also like to thank Mr. Brandon Van Leer and Dr. Jan Ringnalda of Thermo Fischer Scientific for helpful sample preparation advice, Mr. Peter Yurek of Medtronic for performing the x-ray diffraction experiment, Mr. Brian Leigh of Medtronic for performing the ICP-OES analysis, and Ms. Margaret Flury of Medtronic for careful proofreading of this manuscript. Parts of this work were carried out in the Characterization Facility, University of Minnesota, which receives partial support from NSF through the MRSEC program. ROR was supported by the Office of Science, Office of Basic Energy Sciences, Materials Sciences and Engineering Division, under contract no. DE-AC02-05CH11231. DK acknowledges funding by the European Research Council under grant number 771146 (TOUGHIT).

Supplementary materials

Supplementary material associated with this article can be found, in the online version, at doi:10.1016/j.actamat.2019.11.021.

References

[1] C. Suryanarayana, A. Inoue, Bulk Metallic Glasses, CRC Press, 2011.
[2] B. Gludovatz, S.E. Naleway, R.O. Ritchie, J.J. Kruzic, Size-dependent fracture toughness of bulk metallic glasses, Acta Mater. 70 (2014) 198–207.
[3] B. Gludovatz, D. Granata, K.V.S. Thurston, J.F. Löffler, R.O. Ritchie, On the understanding of the effects of sample size on the variability in fracture toughness of bulk metallic glasses, Acta Mater. 126 (2017) 494–506.
[4] W. Chen, H. Zhou, Z. Liu, J. Ketaew, N. Li, J. Yurko, N. Hutchinson, H. Gao, J. Schroers, Processing effects on fracture toughness of metallic glasses, Scr. Mater. 130 (2017) 152–156.
[5] V. Schnabel, B. Nagamani Jaya, M. Köhler, D. Music, C. Kirchlechner, G. Dehm, D. Raabe, J.M. Schneider, Electronic hybridisation implications for the damage–tolerance of thin film metallic glasses, Sci. Rep. 6 (2016) 36556.
[6] C.J. Gilbert, R.O. Ritchie, W.L. Johnson, Fracture toughness and fatigue-crack propagation in a Zr–Ti–Ni–Cu–Be bulk metallic glass, Appl. Phys. Lett. 71 (1997) 476–478.
[7] C.J. Gilbert, V. Schroeder, R.O. Ritchie, Mechanisms for fracture and fatigue-crack propagation in a bulk metallic glass, Metall. Mater. Trans. A 30 (1999) 1739–1753.
[8] S.L. Philo, J.J. Kruzic, Fatigue crack growth behavior of a zr–ti–cu–ni–be bulk metallic glass: Role of ambient air environment, Scr. Mater. 62 (2010) 473–476.
[9] S.L. Philo, J. Heinrich, I. Gallino, R. Busch, J.J. Kruzic, Fatigue crack growth behavior of a $Zr_{58.5}Cu_{15.6}Ni_{12.8}Al_{10.3}Nb_{2.8}$ bulk metallic glass-forming alloy, Scr. Mater. 64 (2011) 359–362.
[10] S.E. Naleway, R.B. Greene, B. Gludovatz, N.K.N. Dave, R.O. Ritchie, J.J. Kruzic, A highly fatigue-resistant Zr-based bulk metallic glass, Metall. Mater. Trans. Part A 44 (2013) 5688–5693.
[11] M.L. Morrison, R.A. Buchanan, P.K. Liaw, B.A. Green, G.Y. Wang, C.T. Liu, J.A. Horton, Four-point-bending-fatigue behavior of the Zr-based Vitreloy 105 bulk metallic glass, Mater. Sci. Eng. A 467 (2007) 190–197.
[12] A. Bharathula, S.W. Lee, W.J. Wright, K.M. Flores, Compression testing of metallic glass at small length scales: effects on deformation mode and stability, Acta Mater. 58 (2010) 5789–5796.
[13] Y.H. Lai, C.J. Lee, Y.T. Cheng, H.S. Chou, H.M. Chen, X.H. Du, C.I. Chang, J.C. Huang, S.R. Jian, J.S.C. Jang, T.G. Nieh, Bulk and microscale compressive behavior of aZr-based metallic glass, Scr. Mater. 58 (2008) 890–893.
[14] Dongchan Jang, Cameron T. Gross, Julia R. Greer, Effects of size on the strength and deformation mechanism in Zr-based metallic glasses, Int. J. Plast. 27 (2011) 858–867.
[15] C.J. Lee, J.C. Huang, T.G. Nieh, Sample size effect and microcompression of Mg65Cu25Gd10 metallic glass, Appl. Phys. Lett. 91 (2007) 161913.
[16] C.Q. Chen, Y.T. Pei, J.T.M. De Hosson, Effects of size on the mechanical response of metallic glasses investigated through in situ tem bending and compression experiments, Acta Mater. 58 (2010) 189–200.
[17] O.V. Kuzmin, Y.T. Pei, C.Q. Chen, J.T.M. De Hosson, Intrinsic and extrinsic size effects in the deformation of metallic glass nanopillars, Acta Mater. 60 (2012) 889–898.
[18] D. Jang, C.T. Gross, J.R. Greer, Effects of size on the strength and deformation mechanism in zr-based metallic glasses, Int. J. Plast. 27 (2011) 858–867.
[19] J. Ding, S. Patinet, Michael L. Falk, Yongqiang Cheng, Evan Ma, Soft spots and their structural signature in a metallic glass, Proc. Natl Acad. Sci. 111 (2014) 14052–14056.
[20] Jian Xu, Evan Ma, Damage-tolerant zr–cu–al-based bulk metallic glasses with record-breaking fracture toughness, J. Mater. Res. 29 (2014) 1489–1499.
[21] T. Fukushige, S. Hata, A. Shimokohbe, A mems conical spring actuator array, J. Microelectromech. Syst. 14 (2005) 243–253.
[22] Z. Wang, L. Yan, Y. Yang, J.F. Li, J. Das, A. Geiler, A. Yang, Y. Chen, V.G. Harris, D. Viehland, Magnetoelectric effect in crystallographically textured batio3 films deposited on ferromagnetic metallic glass foils, J. Appl. Phys. 109 (2011) 034102.
[23] K. Richter, Amorphous Metal Alloy Medical Devices, Google Patents, 2011.
[24] J.F. Löffler, Bulk metallic glasses, Intermetallics 11 (2003) 529–540.
[25] J.H. Tregilgas, Amorphous titanium aluminide hinge, Adv. Mater. Proc. 162 (2004) 40–41.
[26] http://www.liquidmetal.com/wp-content/uploads/2015/12/LM105-Properties.pdf.
[27] W.J. Wright, R.B. Schwarz, W.D. Nix, Localized heating during serrated plastic flow in bulk metallic glasses, Mater. Sci. Eng. A 319–321 (2001) 229–232.
[28] C.A. Schuh, T.G. Nieh, A nanoindentation study of serrated flow in bulk metallic glasses, Acta Mater. 51 (2003) 87–99.
[29] W.J. Wright, R. Saha, W. Nix, Deformation mechanisms of the Zr40Ti14Ni10Cu12Be24 bulk metallic glass, Mater. Trans. 42 (2001) 642–649.
[30] X. Zhao, R.M. Langford, J. Tan, P. Xiao, Mechanical properties of sic coatings on spherical particles measured using the micro-beam method, Scr. Mater. 59 (2008) 39–42.
[31] D. Di Maio, S.G. Roberts, Measuring fracture toughness of coatings using focused-ion-beam-machined microbeams, J. Mater. Res. 20 (2005) 299–302.
[32] Y. Murakami, Stress intensity factors handbook, Elsevier Science Limited (1987).

[33] ASTM E1820-17a, Standard test method for measurement of fracture toughness, Proceedings of the ASTM International, West Conshohocken, PA, 2017.
[34] R. Pippan, S. Wurster, D. Kiener, Fracture mechanics of micro samples: Fundamental considerations (Invited review), Mater. Des. 159 (2018) 252–267.
[35] A. Bharathula, S.-W. Lee, W.J. Wright, K.M. Flores, Compression testing of metallic glass at small length scales: Effects on deformation mode and stability, Acta Mater. 58 (2010) 5789–5796.
[36] B. Chen, T.L. Shi, M. Li, F. Yang, F. Yan, G.L. Liao, Laser welding of annealed Zr55Cu30Ni5Al10 bulk metallic glass, Intermetallics 46 (2014) 111–117.
[37] R.D. Conner, Y. Li, W.D. Nix, W.L. Johnson, Shear band spacing under bending of zr-based metallic glass plates, Acta Mater. 52 (2004) 2429–2434.
[38] C.T. Liu, L. Heatherly, D.S. Easton, C.A. Carmichael, J.H. Schneibel, C.H. Chen, J.L. Wright, M.H. Yoo, J.A. Horton, A. Inoue, Test environments and mechanical properties of Zr-base bulk amorphous alloys, Mater. Trans. A 29 (1998) 1811–1820.
[39] H. Bei, S. Xie, E.P. George, Softening caused by profuse shear banding in a bulk metallic glass, Phys. Rev. Lett. 96 (2006) 105503.
[40] J.W. Hutchinson, Singular behavior at the end of a tensile crack in a hardening material, J. Mech. Phys. Solids 16 (1968) 13–31.
[41] J.R. Rice, G.F. Rosengren, Plane strain deformation near a crack tip in a power-law hardening material, J. Mech. Phys. Solids 16 (1968) 1–12.
[42] R.O. Ritchie, The conflicts between strength and toughness, Nat. Mater. 10 (2011) 817–822.
[43] F.X. Liu, P.K. Liaw, G.Y. Wang, C.L. Chiang, D.A. Smith, P.D. Rack, J.P. Chu, R.A. Buchanan, Specimen-geometry effects on mechanical behavior of metallic glasses, Intermetallics 14 (2006) 1014–1018.
[44] J.-Y. Suh, D.R. Conner, P.C. Kim, M. Demetriou, W. Johnson, Plastic zone formation and fracture of Zr-based bulk metallic glasses, Presented at the Society for Experimental Mechanics Annual Conference Albuquerque New Mexico USA, 2009.